Chemical Physics 361 (2009) 61–67

Contents lists available at ScienceDirect

Chemical Physics

journal homepage: www.elsevier.com/locate/chemphys

Spectra and photophysics of new organic fluorophores: 2,3-Di(phenylethenyl)benzofuran derivatives

Ivan Baraldi [a], Enrico Benassi [a,*], Serena Ciorba [b], Marija Šindler-Kulyk [c], Irena Škorić [c], Anna Spalletti [b,*]

[a] Dipartimento di Chimica, Università di Modena e Reggio Emilia, 41100 Modena, Italy
[b] Dipartimento di Chimica e Centro di Eccellenza Materiali Innovativi Nanostrutturati (CEMIN), Università di Perugia, 06123 Perugia, Italy
[c] Department of Organic Chemistry, Faculty of Chemical Engineering and Technology, University of Zagreb, 10000 Zagreb, Croatia

ARTICLE INFO

Article history:
Received 25 March 2009
Accepted 13 May 2009
Available online 18 May 2009

Keywords:
Absorption and emission spectra
Intramolecular charge transfer states
Distyrylbenzofurans
Fluorophores
Molecular quantum mechanics
Photophysics
Fluorosolvatochromism

ABSTRACT

Conformations, spectra and photophysics of a series of new organic fluorophores, 2,3-distyrylbenzofuran derivatives, have been studied by a combined theoretical and experimental approach. Ground electronic state geometries have been investigated by Hartree-Fock ab initio methods and Density Functional Theory. Electronic spectra have been calculated with the CS INDO S-CI and SDT-CI procedures. Spectral and photophysical behaviour has been investigated by stationary and time-resolved techniques. Solvatochromism of these compounds has been analyzed. The UV–vis absorption spectra of the substituted compounds are very similar, showing a red shift in the series H < Cl < OCH_3 < NH_2 < NO_2. The CS INDO CI analysis of the electronic spectra of all rotamers shows coherence with the prevalent presence of one non-planar conformer. These compounds are very stable and show an intense and structured fluorescence indicating that the emitting state is the same as that reached by absorption, i.e. the $|\pi_H\pi_L^*\rangle$ singlet state. The nitro-derivative behaviour is exceptional if compared to the other compounds since it displays a strong fluorosolvatochromism, due to an intramolecular charge transfer state.

1. Introduction

The design, synthesis and study of new organic fluorophores have attracted our attention because of their potential applications as fluorescent probes in biology and medicine, in analytical and environmental sciences, in dye lasers and in optoelectronics [1,2]. In particular, we have recently found that 2,3- and 2,5-(distyryl)furan [2,*n*-$(St)_2F$, with $n = 3$ or 5], as well as 2,5-(distyryl)thiophene, show all the characteristics of fluorescence probes, such as an intense and structured emission [3,4]. In addition, the rotational isomerism, the properties of the UV–vis absorption spectra and the solvatochromism were accurately investigated for these compounds. It was pointed out that their absorption properties are similar to those of *cis*-α,ω-diphenylpolyenes, particularly regarding the presence of the *cis* peak [5], while their emissions are very different with respect to *all-trans*-α,ω-diphenylpolyenes. All spectroscopic and photophysical results indicated that the same excited electronic state (the $|\pi_H\pi_L^*\rangle$ singlet state) is responsible for both emission and absorption.

Proceeding with our research project on this class of compounds [3–8], this paper deals with the 2,3-distyryl-derivatives of benzofuran (X–BF, with X = H, OCH_3, Cl, NH_2, NO_2), whose structures are reported in Scheme 1. The interaction of the "styryl" moieties with the heterocycle rings is a central point of the present work. The results of the molecular quantum mechanics CS INDO CI calculations [9] on the most stable *EE* conformers and photophysical characterization of these emitting molecules allow the spectral behaviour to be explained.

The observed fluorosolvatochromism for X = NH_2 and NO_2 points to the intramolecular charge transfer (ICT) character of the excited singlet state.

2. Computational and experimental procedures

2.1. Computational

A full geometry optimization at HF ab initio 6-31G* level and at DFT level using 6-31G* basis set and considering B3-LYP functional was employed to obtained the forms of X–BF conformers. The starting points for the geometry optimization were the planar and non-planar geometries of the rotamers. The initial non-planar geometries were obtained twisting the lateral rings by $\pm\pi/6$ rad with respect to the internal axes starting from planar forms. The HF and DFT optimized geometries were submitted to vibrational analysis to investigate whether the convergence points were true ("genuine") energy minima. Gaussian 03 computational package [10] was used in all these calculations.

* Corresponding authors. Tel.: +39 059 2055085; fax: +39 059 373543 (E. Benassi), tel.: +39 075 5855575; fax: +39 075 5855598 (A. Spalletti).
E-mail addresses: baraldi.ivan@unimore.it (I. Baraldi), enrico.benassi@libero.it (E. Benassi), serena.ciorba@virgilio.it (S. Ciorba), marija.sindler@fkit.hr (M. Šindler-Kulyk), iskoric@fkit.hr (I. Škorić), faby@unipg.it (A. Spalletti).

0301-0104/$ - see front matter © 2009 Elsevier B.V. All rights reserved.
doi:10.1016/j.chemphys.2009.05.009

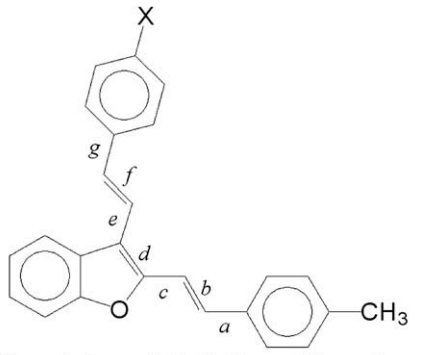

2-(4'-methyl-styryl),3-(4'-X-styryl)benzofuran

X-BF (X = H, Cl, OCH_3, NH_2, NO_2)

Scheme 1. 2-(4′-Methyl-styryl), 3-(4′-X-styryl)benzofuran X–BF (X = H, Cl, OCH_3, NH_2, NO_2).

As introduced in Section 1, the calculations of the excited electronic singlet states and, in consequence, the $S_0 \rightarrow S_n$ absorption spectra of the "stable" rotamers were performed with the CS INDO CI methods that treats valence-shell states only [9]. The optimized geometries of the non-planar conformers in the ground electronic state, as obtained from HF ab initio level and DFT calculations, were used in the CS INDO CI calculations. Details of the CS INDO calculations are not reported below, because they coincide with those previously described for related compounds [11–13]. The configuration interactions were estimated both in the singly-excited (S-CI) and in multiple excitation (SDT-CI) schemes. A MO active space in the CI calculations included all the MOs having a significant π character. Some crucial full MO calculations were also performed. All these theoretical analyses refer to the molecules in the gas phase. During the presentation of the results and their discussion, as well as in the classification of configurations, the frontier orbitals HOMO and LUMO will be indicated with *H* and *L*, respectively.

The radius of the cavity occupied by the solute molecule in the solvent within Onsager's model was calculated in the case of the nitro-derivative for all the solvents used in the experimental measurements with the following procedure: for each solvent, a full geometry optimization of the solvent molecular structure, both at HF/6-311G** and at B3-LYP/6-311G** level of the theory, was obtained. The solvent probe radius was calculated using the internal volume within a contour isosurface of 1×10^{-3} electrons/bohr^3 density and assuming a spherical geometry. Using both the HF and the DFT optimized geometry of the most stable conformer, the cavity volume was calculated by integration of the solvent accessible surface. Then, the cavity radius of the most stable conformer was reached assuming a spherical geometry, as provided by the Onsager's model. A mean value was then utilized.

2.2. Experimental

About synthetic methodologies and purification of these products, see Ref. [8]. The synthesis of NH_2–BF was performed by reduction of the NO_2–BF derivative (see Supplementary materials).

A Perkin–Elmer Lambda 800 spectrophotometer was used for the absorption measurements. The experimental oscillator strength of the principal band (f_p) and that of the "*cis* peak" (f_c) were derived by $f = \frac{4.39\times10^{-9}}{n} \int \varepsilon(\overline{\nu})d\overline{\nu}$ [14], considering the refraction index $n \cong 1$.

The fluorescence spectra were measured by a Spex Fluorolog-2 F112AI spectrofluorimeter. Dilute solutions (absorbance less than 0.1 at the excitation wavelength, λ_{exc}) were used for fluorimetric measurements. 9,10-diphenylanthracene in de-aerated cyclohexane was used as fluorimetric standard ($\Phi_F = 0.90$ [15]). Fluorescence lifetimes were measured by an Edinburgh Instrument 199S spectrofluorimeter, using the single photon counting method.

All measurements were performed at room temperature in *n*-hexane (H) and acetonitrile (ACN). For a detailed solvent effect, also toluene, isopentane (IP), methylcyclohexane (MCH), carbon tetrachloride (CCl_4), ethyl acetate (EtAc), bromo-naphthalene (BrN), 1,2-dichloroethane (DCE), ethanol (EtOH), dimethylsulfoxide (DMSO) and acetone were used. All solvents used were spectroscopic grade from Fluka.

The fluorescence quantum yields and lifetimes were measured in de-aerated solutions by purging with nitrogen.

The triplet state was investigated by nanosecond laser flash photolysis using a Continuum Surelite II Nd:YAG laser. The quantum yields of singlet oxygen production (ϕ_Δ) in the presence of air were obtained by measuring its phosphorescence in fluid solution with a germanium diode using phenalenone as standard ($\phi_\Delta = 0.97$ [16]).

The parameters reported in the Tables are averages of at least three independent measurements with mean deviation of *ca.* 10%. The lifetimes under 0.5 ns, at the limits of the instrumental resolution, can be affected by larger errors.

3. Results and discussion

3.1. Conformations and rotational isomerism

A rotational isomerism can be hypothesized for the X–BF compounds as shown in Scheme 2.

The results of the quantum mechanical calculations on the conformers of Scheme 2 are reported in Table 1, in which the total energies are referred to the non-planar A conformer. Bond length alternation (*BLA*) is also reported. The computed energies indicate that the conformations are not planar and that the A and C non-planar conformers are more stable than B and D, the latter being the most destabilized. An example of conformation of A rotamer after HF optimization is reported in Fig. 1, showing that the 2-styryl group is *quasi* "planar" with respect to the benzofuran ring, while the 3-styryl group is angulated. The "phenyl" twisting angles found after the optimization procedures are in the range 14–28 degrees at HF level and 1–13 degrees with the DFT/B3LYP calculations, where the main torsion angle is referred to the 3-styryl group. As a matter of fact, in Refs. [3,7], the DFT/B3LYP calculations generally provide more planar conformations than the HF ones for this kind of molecules. Such behaviour can be derived also from

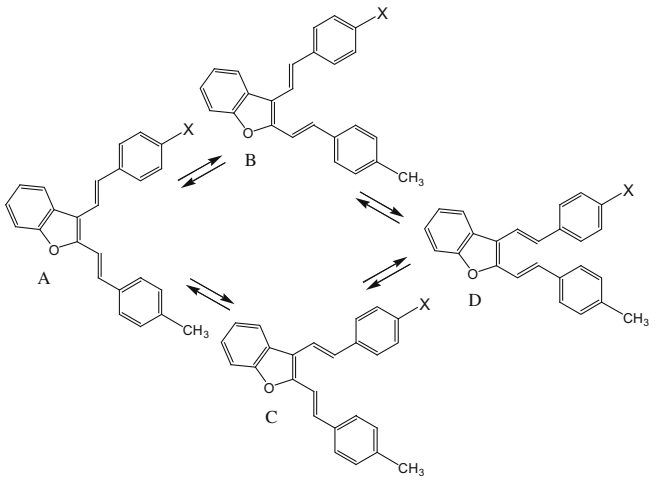

Scheme 2.

Table 1
Calculated energy difference and *BLA* among conformers of H–BF.

	A non-planar conformation	B non-planar conformation	C non-planar conformation	D non-planar conformation
ΔE/(kJ mol^{-1})				
HF[a]	0	7.060	−0.077	16.689
DF[b]	0	8.581	2.988	19.642
BLA/Å				
HF[c]	0.126	0.128	0.128	0.135
DF[c]	0.082	0.085	0.084	0.090

[a] HF ab initio calculations at 6-31G* level.
[b] DFT calculations with 6-31G* basis set considering B3-LYP functional.
[c] $BLA = \frac{1}{3}\left[\left(\frac{a+g}{2}+c+e\right)-(b+d+f)\right]$ (bonds are indicated in Scheme 1). The values are referred to the most stable forms.

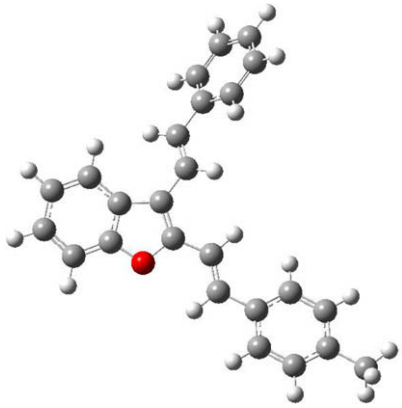

Fig. 1. Conformation of the A rotamer after HF full geometry optimization at 6-31G* level.

BLA data of Table 1. The *BLA*(HF) coincides with those of the standard polyenes, while the *BLA*(DFT) is significantly smaller, probably because of a DFT overestimation of the conjugation. These findings are in agreement with previous results on conformations of 2,*n*-distyrylfurans [3].

Using a mean value of 7.0 kJ/mol and 20.0 kJ/mol as destabilization energies, of B and D, respectively, in comparison with A, the Boltzmann factors indicate an abundance of B of about 5% and a negligible presence of D at room temperature. The relative abundances of the conformers were estimated neglecting the entropy terms. Similar entropies for different conformers were obtained at 298.15 K and 1 atm by the DFT calculations.

The vibrational analysis performed on A, B, C and D non-planar optimized geometries of H–BF, excluding the torsion of the methyl group, gave all positive frequencies, indicating the presence of "genuine" energy minima.

In the following the conformational study of X–BFs has been performed for A and C rotamers only, being the most stable species of H–BF.

Table 2 presents the ground states energies and the *BLA* values, obtained at HF and DFT levels, for these two non-planar conformers of the X–BFs. For the amino-, and even more for the nitro-derivative, the *BLA* values are lower than those calculated for the other compounds. This behaviour, that indicates a larger conjugation in these two compounds, could be due to an increased ICT character of their ground state. All substituents adopt a planar conformation with respect to the benzene ring.

3.2. UV–vis absorption spectra

Fig. 2a–e present the UV–vis absorption and fluorescence emission spectra of the X–BFs, in the order X = H (a), Cl (b), OCH_3 (c), NH_2 (d) and NO_2 (e), in *n*-hexane and acetonitrile at room temperature and Table 3 reports the spectral properties of the first and second absorption bands.

Table 2
Calculated energy differences and *BLA* among conformers of X–BF.

X		A non-planar conformation	C non-planar conformation
ΔE/(kJ mol^{-1})			
Cl	HF[a]	0	0.204
	DF[b]	0	3.054
OCH_3	HF[a]	0	−0.433
	DF[b]	0	2.350
NH_2	HF[a]	0	0.155
	GF[b]	0	2.551
NO_2	HF[a]	0	1.176
	DF[b]	0	4.281
BLA/Å			
Cl	HF[c]	0.126	0.128
	DF[c]	0.081	0.084
OCH_3	HF[c]	0.126	0.128
	DF[c]	0.081	0.084
NH_2	HF[c]	0.125	0.126
	DF[c]	0.079	0.081
NO_2	HF[c]	0.123	0.080
	DF[c]	0.077	0.080

[a] See footnotes of Table 1.
[b] See footnotes of Table 1.
[c] See footnotes of Table 1.

For the derivatives with X = H, Cl and OCH_3, the first (principal) band maxima are found at 371–376 nm; the band is rather strong ($f_p \cong 0.82$–0.83) and shows a partial resolved vibrational structure with maxima corresponding to the transitions from the vibrational level $v = 0$ of the ground state to the $v' = 2$ level of S_1. On the base of the Franck-Condon principle, we conclude that this electronic excitation might cause a significant change of the molecular geometry in the excited state in agreement with the significant Stokes shifts ($\Delta\tilde{\nu}_{S,max}$) found for all the compounds in *n*-hexane (see below, Table 6). Because of the perturbation of the benzofuran ring, a red shift of about 12 nm is observed in the principal band, with respect to that observed for 2,3-$(St)_2F$ [3]. The second electronic band, of strong intensity ($f_c \cong 0.79$–0.92), has two maxima. This is the analogous of the second absorption band of 2,3-$(St)_2F$, *cis* peak, found at 275 nm, and is red shifted of about 20 nm, much more than the principal band.

The UV–vis absorption spectra of NH_2–BF and NO_2–BF in *n*-hexane are red shifted of about 20–40 nm with respect to the first three derivatives. The principal band is relatively strong ($f_p \cong 0.70$) and shows a reduced vibrational structure. The second electronic band, of similar intensity, presents two maxima.

The CS INDO CI calculated energies for the non-planar A and C conformers of H–BF were found to be very similar (Tables 1S and 2S in Supplementary materials).

Table 3
Absorption data (wavelength, λ_{abs}^{max}, energy of the maximum, ΔE, and oscillator strength, *f*) from experimental spectra of X–BFs in *n*-hexane.

X	1st band			2nd band		
	λ_{abs}^{max}/nm	ΔE/eV	f_p	λ_{abs}^{max}/nm	ΔE/eV	f_c
H	371	3.342	0.817	302	4.106	0.786
Cl	375	3.307	0.834	305	4.066	0.869
OCH_3	376	3.298	0.830	303	4.092	0.918
NH_2	382	3.246	0.694	311	3.987	0.874
NO_2	411	3.017	0.698	334	3.716	0.707

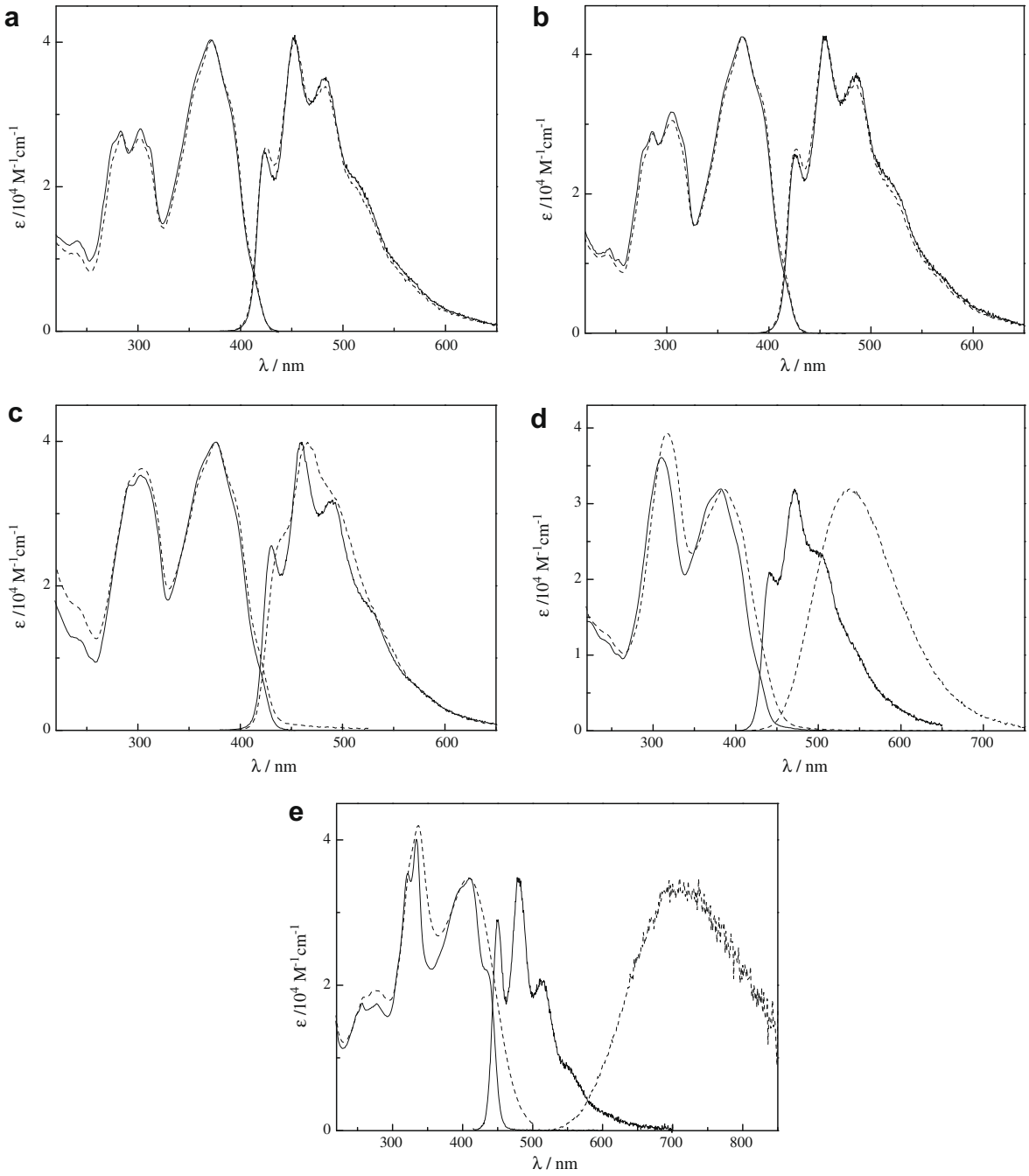

Fig. 2. UV–vis absorption and fluorescence emission spectra of X–BFs, in the order X = H (a), Cl (b), OCH_3 (c), NH_2 (d) and NO_2 (e), in *n*-hexane (solid) and acetonitrile (dash; normalized to the spectrum in *n*-hexane) at room temperature.

In Table 4, we summarize the CS INDO S-CI and SDT-CI results for the $S_0 \rightarrow S_n$ absorption spectra of the A conformers of the X–BF derivatives, as well as those obtained with DFT non-planar geometries. The data of the first three electronic states are reported together with the magnitude (d) of the calculated permanent electric dipole moment vector (**d**). Tables reporting data extended to the first ten electronic states for all the investigated compounds are reported in Supplementary materials.

The first two calculated transitions always are in good agreement with the two experimental absorption bands (see Table 3 and Fig. 2). The $S_0 \rightarrow S_n$ transitions are essentially of $\pi \rightarrow \pi^*$ nature, generally allowed or moderately allowed and polarized in the "molecular plane". Particularly, they are expected to be influenced by the "polyenic" character, therefore some transitions are polarized along the polyene axis (molecular "long" axis) and others along a "perpendicular" axis (molecular "short" axis). The $S_0 \rightarrow S_1$ transition, "long" axis polarized, is responsible for the first absorption band, while the $S_0 \rightarrow S_2$ transition, "short" axis polarized, is responsible for the second band, the "*cis* peak". Such polarizations are confirmed by the CS INDO CI results on the direction of the electronic transition moments. In particular, the calculation of the angle between the S_1–S_2 transition moments gives about 80° for the A conformations.

Generally the CS INDO CI results for the non-planar B and D conformers show an oscillator strength of the $S_0 \rightarrow S_2$ transition much higher than that of the $S_0 \rightarrow S_1$ one. This fact, in disagreement with the experimental finding, excluded a significant presence of the B and D rotamers at room temperature for all the

Table 4
CS INDO S-CI and SDT-CI results for the $S_0 \rightarrow S_n$ absorption spectra of the A conformer (DFT optimized geometry) of X–BFs.

X	Transition $S_0 \rightarrow S_n$	S-CI			SDT-CI		
		ΔE/eV	$f_{(0\text{-}n)}$	d/D	ΔE/eV	$f_{(0\text{-}n)}$	d/D
H	$n = 0$	–	–	0.842	–	–	0.695
	1	3.344	0.992	1.462	3.247	0.815	1.278
	2	4.110	0.702	3.611	4.098	0.781	5.438
Cl	$n = 0$	–	–	2.193	–	–	2.134
	1	3.305	0.914	2.238	3.421	0.834	3.395
	2	4.069	0.952	5.179	4.108	0.870	4.573
OCH_3	$n = 0$	–	–	2.159	–	–	1.927
	1	3.301	0.905	1.126	3.478	0.829	1.181
	2	4.089	0.948	4.842	4.303	0.916	6.433
NH_2	$n = 0$	–	–	2.414	–	–	2.595
	1	3.245	0.745	3.991	3.501	0.700	4.586
	2	3.982	0.901	2.602	4.085	0.872	2.860
NO_2	$n = 0$	–	–	9.278	–	–	8.864
	1	2.997	0.751	15.327	3.270	0.700	26.379
	2	3.709	0.874	18.224	3.829	0.710	18.269

investigated compounds, as expected on the base of the calculated Boltzmann's factors.

SDT-CI wavefunctions analysis of the A conformation in the case of H–BF shows that the polyexcited configurations have an appreciable role on the electronic spectrum of this molecule. The energy of the ground electronic state is less influenced than the excited states, giving a lower transition energy with respect to the S-CI calculations. The S_1 state is characterized by the $|HL\rangle \equiv |\pi_H \pi_L^*\rangle$ singly excited configuration, while S_2 is characterized by the singly excited $|HL+1\rangle$ and the doubly excited $|H^0L^2\rangle$ configurations. The MOs involved in such transitions, H, L and L+1, have the same characteristic of the MOs involved in the polyenic chains, even if H results to be more delocalized, whereas L and $L+1$ appear more localized, in contrast with those of the polyenic chains.

Also for Cl–BF (Table 4), the first excited singlet state is essentially characterized by the $|HL\rangle \equiv |\pi_H \pi_L^*\rangle$ singly excited configuration, whereas the second excited singlet state, is characterized, principally, by the singly excited $|HL+1\rangle$ configuration. In the case of the methoxy- and amino-derivatives $|HL+2\rangle$ and $|H-1L\rangle$ configurations also contribute to the second excited state, while for NO_2–BF both S_1 and S_2 are characterized by the $|HL\rangle \equiv |\pi_H \pi_L^*\rangle$ and $|HL+1\rangle$ singly excited configurations.

The MOs involved in such transitions appear as delocalized on the whole molecular structure with the exception of L in the NO_2–BF that resulted localized on the nitro-group. In the last case the presence of the $|HL\rangle$ configuration in both S_1 and S_2 indicates a significant charge transfer character. It is also interesting to note that, contrary to the other compounds, the first two singlet excited states of NO_2–BF have large dipole moments, more than doubled with respect to that of the ground state.

3.3. Fluorescence emission spectra and photophysics

Table 5 reports the spectral behaviour (maxima wavelengths and vibronic progressions of the absorption and emission spectra and the Stokes-shifts) of the studied compounds in *n*-hexane at room temperature. The Stokes-shifts were calculated by both the maxima, $\Delta\tilde{\nu}_{S,max}$, and the 0,0 transition, $\Delta\tilde{\nu}_{S,00}$, in the absorption and emission spectra of Fig. 2.

In Table 6, the fluorimetric parameters (fluorescence quantum yield, Φ_F, lifetime, τ_F, and kinetic fluorescence constant, k_F) in *n*-hexane and acetonitrile at room temperature are reported. The main pathway for the deactivation of the singlet excited states was fluorescence with the exception of the nitro-derivative.

The emission spectra in non polar solvent, shown in Fig. 2, are intense and display a well resolved vibrational structure (vibronic progression of about 1400 cm^{-1}), better than that observed in the principal absorption band. As a general rule, such spectral behaviour is connected to a larger planarity and rigidity of the emitting state with respect to the S_0 ground state. Similarly to the absorption, the emission spectra show, as expected, a red shift with respect to the unsubstituted H–BF, which increases on going from the chlorine- to the nitro-derivative.

The high emission quantum yields and fluorescence lifetimes of few nanoseconds (with the exception of the nitro-derivative) are little affected by the polarity of the solvent (see below) and lead to fluorescence rate constants of the order of 10^8 s^{-1}, a value characteristic of allowed transitions, in agreement with the small $\Delta\tilde{\nu}_{S,00}$ found for all these compounds (see Table 5).

The X–BFs have been reported to be very stable under irradiation (quantum yields of few percents have been determined for the *trans* → *cis* photoisomerization process only in the case of the unsubstituted H–BF and its Cl-derivative [8]).

The reduction in the fluorescence quantum yield and lifetime in the case of the nitro-derivative has been previously explained by an efficient competitive $S_1 \rightarrow T_1$ intersystem crossing that leads to a non-reactive triplet state (a quantum yield of singlet oxygen production, $\Phi_\Delta = 0.55$ in *n*-hexane, has been reported [8]), as well documented for similar compounds [17].

Table 5
Spectral behaviour of the X–BFs in *n*-hexane at room temperature.[a]

X	λ_{abs}^{max}/nm	$\Delta\tilde{\nu}_{abs}$/cm^{-1}	λ_F^{max}/nm	$\Delta\tilde{\nu}_F$/cm^{-1}	$\Delta\tilde{\nu}_{S,max}$/$cm^{-1}$	$\Delta\tilde{\nu}_{S,00}$/cm^{-1}
H	371, 390^{sh}, 412^{sh}	1310	424, 452, 483	1440	4830	690
Cl	375, 392^{sh}, 416^{sh}	1160	426, 454, 486	1450	4640	560
OCH_3	362^{sh}, 376, 394^{sh}, 418^{sh}	1220	430, 459, 491	1450	4810	670
NH_2	367^{sh}, 382, 402^{sh}, 430^{sh}	1300	442, 472, 503	1440	4990	630
NO_2	391^{sh}, 411, 435^{sh}	1290	450, 480, 514	1390	3500	770

[a] The underlined wavelengths refer to the maxima.

Table 6
Fluorimetric parameters for the X–BFs in de-aerated *n*-hexane and acetonitrile at room temperature.

X	*n*-Hexane			Acetonitrile		
	Φ_F	τ_F/ns	$k_F/10^8\ s^{-1}$	Φ_F	τ_F/ns	$k_F/10^8\ s^{-1}$
H	0.67	2.6	2.6	0.56	2.4	2.3
Cl	0.72	3.1	2.3	0.43	1.9	2.3
OCH_3	0.74	3.1	2.4	0.70	3.2	2.2
NH_2	0.54	3.3	1.6	0.58	4.2	1.4
NO_2	0.04	0.2	2.0	0.02	0.2	1.0

The fluorescence spectrum does not depend on λ_{exc} and the excitation spectrum well overlaps the absorption for all the five compounds. These evidences, together with the observed monoexponential fluorescence decays, point to the presence of a prevalent emissive species, in agreement with the theoretical calculations.

3.4. Solvent effects

The polarity of the solvent does not generally affect the shape and the position of the absorption and emission spectra, neither the fluorescence quantum yields nor lifetimes for the compounds where X = H, Cl and OCH_3 in ACN (as shown in Fig. 2 and Table 6). On the contrary, for X = NH_2, and even more for X = NO_2, a significant red shift of the emission spectrum is observed, accompanied by modest changes in the absorption spectrum (only an enlargement of the red tail is observed in Fig. 2e for the nitro-derivative). This behavior leads to a huge increase of the Stokes shifts in ACN for these two compounds ($\Delta\tilde{\nu}_{S,max} = 7400\ cm^{-1}$ for X = NH_2 and 10,300 cm^{-1} for X = NO_2), where the presence of CT transitions is expected.

A more extended study of the solvent effect on the spectral properties and fluorescence quantum yield and lifetime was then carried out in the case of the nitro-derivative. The results obtained in twelve solvents of different polarity and polarizability are shown in Fig. 3 and collected in Tables 7 and 8.

The red shift of the emission spectrum is well related to the increase of the solvent polarity as well as to the loss of vibronic structure. In fact in polar solvent the fluorescence spectrum looks like a very large bell-shaped band.

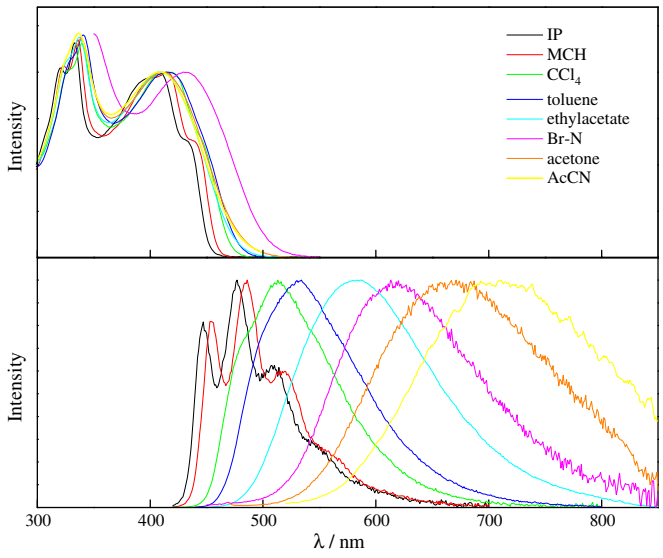

Fig. 3. Solvent effect on the absorption and emission spectra of NO_2–BF at room temperature.

Table 7
Spectral behaviour of NO_2–BF in solvent of different relative dielectric constant (ε) at room temperature.

Solvent	ε	λ_{abs}^{max}/nm	λ_F^{max}/nm	$\Delta\tilde{\nu}_{S,max}/cm^{-1}$	$\Delta\tilde{\nu}_{S,00}/cm^{-1}$
IP	1.84	393^{sh}, 408, 433^{sh}	447, 477, 508	3550	720
H	1.88	391^{sh}, 411, 435^{sh}	450, 480, 514	3500	770
MCH	2.02	398^{sh}, 414, 439^{sh}	454, 486, 517	3580	750
CCl_4	2.24	407^{sh}, 419, 445^{sh}	485, 513, 543	4370	1850
Toluene	2.38	415	533	5340	
BrN	4.768	432	620	7020	
EtAc	6.05	410	583	7240	
DCE	10.37	418	666	8910	
Acetone	20.7	412	671	9370	
EtOH	24.55	410	605	7860	
ACN	35.94	410	710	10,300	
DMSO	46.45	425	715	9540	

Table 8
Photophysical properties of NO_2–BF in solvents of different static refractive index (n) and polarizability (α) at room temperature.

Solvent	n	α	Φ_F[a]	τ_F[a]/ns	$k_F/(10^8\ s^{-1})$	Φ_Δ	$k_{ISC}/(10^9\ s^{-1})$
ACN	1.3441	0.212	0.02	0.2	1.0		
IP	1.3537	0.217	0.03	0.2	1.0	0.66	$\geqslant 3.3$
Acetone	1.3587	0.220	0.02	0.5	0.4		
EtOH	1.3588	0.220	0.004	$\leqslant 0.2$	$\geqslant 0.2$		
EtAc	1.3724	0.227	0.48	3.2	1.5		
H	1.3749	0.228	0.04	0.2	2.0	0.55	$\geqslant 2.8$
MCH	1.4262	0.256	0.07	0.4	1.8	0.48	$\geqslant 1.2$
DCE	1.4448	0.266	0.08	0.8	1.0		
CCl_4	1.4601	0.274	0.26	1.1	2.4		
DMSO	1.4793	0.284	0.17	0.8	2.1		
Toluene	1.4969	0.293	0.34	1.8	1.9		
BrN	1.6570	0.368	0.41	2.9	1.4		

[a] Means in aerated solutions.

The occurrence of this fluorosolvatochromism affects the Stokes shifts that remain roughly the same for the first three solvents with relative dielectric constant ε in the range 1.8–2.0 (Table 7) but increase with ε reaching high values (about 10,000 cm^{-1}) in ACN and DMSO.

The increase of the fluorescence quantum yield observed on increasing the polarizability (α) of the solvent (with the exception of ethylacetate, see Table 8) is not accompanied by a parallel increase of the fluorescence rate constant that remains around $10^8\ s^{-1}$. At this stage of the work, this effect can be tentatively explained by changes in the relative position of the lowest singlet and triplet states of different nature induced by the solvent polarizability that therefore might cause a decrease of the ISC rate constant (k_{ISC}) in solvents of high α. If this is the case, a decrease of Φ_{ISC} (and then Φ_Δ) on increasing the solvent polarizability should be observed. Unfortunately, we succeeded in measuring Φ_Δ in the case of three solvents (IP, H and MCH) only. In fact, revealing the low phosphorescence intensity from the singlet oxygen in the presence of the sensitizer fluorescence is difficult, particularly when it is red-shifted as far as 700–1000 nm. In any case, the observed trend of Φ_Δ and the calculated k_{ISC} (both parameters increase with α) is in agreement with the tentative interpretation.

The large fluorescence shift shown in Fig. 3, typical of states with large CT character [18,19], could imply that stabilization of the state reached by absorption in polar solvents leads to a structure of large ICT character or a new state of different conformation is produced having the NO_2- or NO_2-phenyl-group twisted by 90° ("twisted intramolecular charge transfer", TICT process) [18,20,21]. At this stage of the work we have no clear evidence for the formation of this new state.

To better clarify the nature of the involved excited states, a deeper investigation implying the use of ultrafast techniques (in absorption and emission) is being planned.

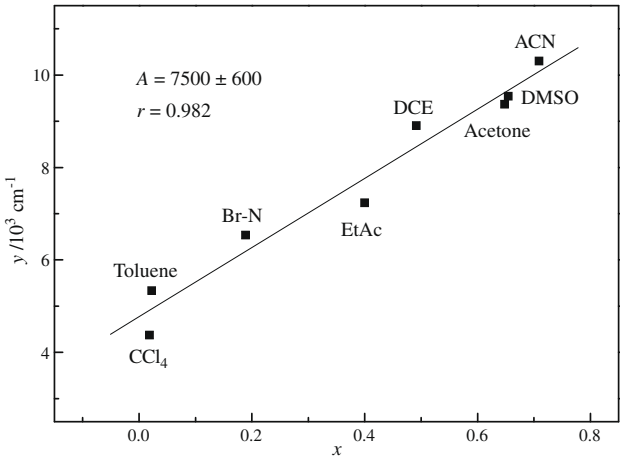

Fig. 4. Plot of spectral shifts in non-protic solvents of different polarity, according to Eq. (1).

An attempt to obtain information on the changes of dipole moment under excitation ($\Delta d \equiv d_e - d_g$) from the experimental results on solvatochromism, was performed by using the Eq. (1):

$$\nu_{ass} - \nu_{em} = (\delta_{ass} + \delta_{em}) + \frac{2(d_e - d_g)^2}{hca^3}\left(\frac{\varepsilon - 1}{\varepsilon + 2} - \frac{n^2 - 1}{n^2 + 2}\right) \quad (1)$$

where $\nu_{ass} - \nu_{em}$ is the Stokes shift (in cm^{-1}), δ_{ass} and δ_{em} are the difference in the vibrational energy (in cm^{-1}) of the molecule in the excited and ground state for absorption and emission, respectively, h is Planck's constant (in erg × s), c is the speed of light in vacuum (in cm s^{-1}), a is the cavity radius within Onsager's model (in cm), ε is the relative dielectric constant and n the static refractive index of the solvent [22,23]. Eq. (1) may be written as:

$$y = Ax + B \quad (2)$$

where $y \equiv \nu_{ass} - \nu_{em}$, $x = f(\varepsilon) - f(n^2) \equiv \left(\frac{\varepsilon-1}{\varepsilon+2} - \frac{n^2-1}{n^2+2}\right)$, $A \equiv \frac{2(d_e-d_g)^2}{hca^3}$, and $B \equiv (\delta_{ass} + \delta_{em})$. A linear trend is found by plotting the spectral data of Table 7 according to Eq. (2) (Fig. 4). The protic solvent and those with dielectric constant smaller than 2.2 not included. From the slope A and using a computed cavity radius of 8.55 Å, a value of 21.6 D was obtained for Δd. This value can be considered in a reasonable agreement with the SDT-CI computed value (17.515 D, Table 4).

4. Conclusions

The main results of the present combined theoretical and experimental approaches led to the following conclusions:

- The photophysical and spectral behaviour points to a largely prevalent conformation for each compound. This is in agreement with the calculations showing that the most stable and abundant form of X–BFs is the A (*trans–trans*) rotamer, accompanied by a smaller amount of C. Moreover, the analysis of the "*cis* peak" is coherent with the presence of A and C.
- The DFT calculations on conformations give smaller *BLA* values and more planar and conjugated structures than those obtained by using the HF methodology.
- The calculated two first $\pi\pi^*$ allowed electronic transitions of the five benzofurans are in agreement with the two bands in the experimental absorption spectra.
- The fluorescence emission spectra and photophysics show that the emitting state is the same as the absorbing $|\pi_H\pi_L^*\rangle$ singlet state.
- The fluorescence spectrum of the nitro-derivative is markedly sensitive to the solvent polarity, as expected on the base of the large increase of the dipole moment on excitation, as obtained by calculations. This increase was nicely confirmed by the analysis of the experimental fluorosolvatochromism, typical of ICT in the excited state.

Acknowledgements

The authors are grateful to Professors Fabio Momicchioli and Ugo Mazzucato for many helpful discussions. This work was supported by Grants from the University of Perugia and the Ministry of Science, Education and Sports of the Republic of Croatia (Grant No. 125-0982933-2926).

Appendix A. Supplementary material

Supplementary data associated with this article can be found, in the online version, at doi:10.1016/j.chemphys.2009.05.009.

References

[1] J.R. Lakowicz, Principle of Fluorescence Spectroscopy, third ed., Springer, Singapore, 2006.
[2] B. Valeur, Molecular Fluorescence – Principles and Applications, Wiley-VCH, Weinheim, 2002.
[3] I. Baraldi, E. Benassi, S. Ciorba, M. Šindler-Kulyk, I. Škorić, A. Spalletti, Chem. Phys. 353 (2008) 163.
[4] G. Ginocchietti, G. Galiazzo, U. Mazzucato, A. Spalletti, Photochem. Photobiol. Sci. 4 (2005) 547.
[5] I. Baraldi, E. Benassi, A. Spalletti, Spectrochim. Acta 71A (2008) 543.
[6] I. Škorić, I. Flegar, Ž. Marinić, M. Šindler-Kulyk, Tetrahedron 62 (2006) 7396.
[7] I. Baraldi, G. Ginocchietti, U. Mazzucato, A. Spalletti, Chem. Phys. 337 (2007) 168.
[8] I. Škorić, S. Ciorba, A. Spalletti, M. Šindler-Kulyk, J. Photochem. Photobiol. A: Chem. 202 (2009) 136.
[9] F. Momicchioli, I. Baraldi, M.C. Bruni, Chem. Phys. 82 (1983) 229.
[10] M.J. Frisch, G.W. Trucks, H.B. Schlegel, G.E. Scuseria, M.A. Robb, J.R. Cheeseman, J.A. Montgomery Jr., T. Vreven, K.N. Kudin, J.C. Burant, J.M. Millam, S.S. Iyengar, J. Tomasi, V. Barone, B. Mennucci, M. Cossi, G. Scalmani, N. Rega, G.A. Petersson, H. Nakatsuji, M. Hada, M. Ehara, K. Toyota, R. Fukuda, J. Hasegawa, M. Ishida, T. Nakajima, Y. Honda, O. Kitao, H. Nakai, M. Klene, X. Li, J.E. Knox, H.P. Hratchian, J.B. Cross, C. Adamo, J. Jaramillo, R. Gomperts, R.E. Stratmann, O. Yazyev, A.J. Austin, R. Cammi, C. Pomelli, J.W. Ochterski, P.Y. Ayala, K. Morokuma, G.A. Voth, P. Salvador, J.J. Dannenberg, V.G. Zakrzewski, S. Dapprich, A.D. Daniels, M.C. Strain, O. Farkas, D.K. Malick, A.D. Rabuck, K. Raghavachari, J.B. Foresman, J.V. Ortiz, Q. Cui, A.G. Baboul, S. Clifford, J. Cioslowski, B.B. Stefanov, G. Liu, A. Liashenko, P. Piskorz, I. Komaromi, R.L. Martin, D.J. Fox, T. Keith, M.A. Al-Laham, C.Y. Peng, A. Nanayakkara, M. Challacombe, P.M.W. Gill, B. Johnson, W. Chen, M.W. Wong, C. Gonzalez, J.A. Pople, Gaussian 03, Revision B.04, Gaussian Inc., Pittsburgh PA, 2003.
[11] I. Baraldi, A. Spalletti, D. Vanossi, Spectrochim. Acta 59A (2003) 75.
[12] I. Baraldi, A. Carnevali, F. Momicchioli, G. Ponterini, Chem. Phys. 160 (1992) 85.
[13] I. Baraldi, A. Carnevali, F. Momicchioli, G. Ponterini, Spectrochim. Acta 49A (1993) 471.
[14] J.B. Birks, Photophysics of Aromatic Molecules, Wiley-Interscience, London, 1970, p. 51, Eq. 3.49.
[15] G. Bartocci, F. Masetti, U. Mazzucato, A. Spalletti, I. Baraldi, F. Momicchioli, J. Phys. Chem. 91 (1987) 4733.
[16] R. Schmidt, C. Tanielian, R. Dunsbach, C. Wolff, J. Photochem. Photobiol. A: Chem. 79 (1994) 11.
[17] H. Görner, F. Elisei, U. Mazzucato, G. Galiazzo, J. Photochem. Photobiol. A: Chem. 43 (1988) 139.
[18] Z.R. Grabowski, K. Rotkiewicz, W. Rettig, Chem. Rev. 103 (2003) 3899, and references therein.
[19] I. Baraldi, G. Brancolini, F. Momicchioli, G. Ponterini, D. Vanossi, Chem. Phys. 288 (2003) 309.
[20] E. Abraham, J. Oberlé, G. Jonusauskas, R. Lapouyade, C. Rullière, Chem. Phys. 214 (1997) 409.
[21] S. Marguet, J.C. Mialocq, P. Millie, G. Berthier, F. Momicchioli, Chem. Phys. 160 (1992) 265.
[22] E.G. McRae, J. Phys. Chem. 61 (1957) 562.
[23] S. Bruni, E. Cariati, F. Cariati, F.A. Porta, S. Quici, D. Roberto, Spectrochim. Acta 57A (2001) 1417. and references therein.